Meteoritics & Planetary Science 41, Nr 10, 1425–1436 (2006)
Abstract available online at http://meteoritics.org

Impact craters in the northern hemisphere of Mars: Layered ejecta and central pit characteristics

Nadine G. BARLOW

Department of Physics and Astronomy, Northern Arizona University, NAU Box 6010, Flagstaff, Arizona 86011–6010, USA
E-mail: nadine.barlow@nau.edu

(Received 20 October 2005; revision accepted 20 May 2006)

Abstract–Mars Global Surveyor (MGS) and Mars Odyssey data are being used to revise the *Catalog of Large Martian Impact Craters.* Analysis of data in the revised catalog provides new details on the distribution and morphologic details of 6795 impact craters in the northern hemisphere of Mars. This report focuses on the ejecta morphologies and central pit characteristics of these craters. The results indicate that single-layer ejecta (SLE) morphology is most consistent with impact into an ice-rich target. Double-layer ejecta (DLE) and multiple-layer ejecta (MLE) craters also likely form in volatile-rich materials, but the interaction of the ejecta curtain and target-produced vapor with the thin Martian atmosphere may be responsible for the large runout distances of these ejecta. Pancake craters appear to be a modified form of double-layer craters where the thin outer layer has been destroyed or is unobservable at present resolutions. Pedestal craters are proposed to form in an ice-rich mantle deposited during high obliquity periods from which the ice has subsequently sublimated. Central pits likely form by the release of vapor produced by impact into ice-soil mixed targets. Therefore, results from the present study are consistent with target volatiles playing a dominant role in the formation of crater morphologies found in the Martian northern hemisphere.

INTRODUCTION

Background

Martian impact craters display a variety of ejecta and interior features which differ from those seen on dry and atmosphere-free bodies like the Moon. These features were first clearly revealed in Viking Orbiter images and included layered (or "fluidized") ejecta patterns and a high number of craters with central pits. To explain these different crater morphologies, attention immediately focused on the ways in which the Martian environment differs from the Moon, specifically the thin Martian atmosphere and the possible presence of near-surface volatile reservoirs.

Fresh Martian impact craters exhibit a wide variety of ejecta morphologies (Barlow et al. 2000). The most common are the layered ejecta morphologies, which have been classified as single-layer ejecta (SLE), double-layer ejecta (DLE), or multiple-layer ejecta (MLE) based on the number of identifiable ejecta layers surrounding the crater (1, 2, or 3+, respectively). Numerous studies based on Viking image analysis have shown that craters with these morphologies have the following characteristics:

1. SLE is the most common ejecta morphology over the entire Martian surface (Mouginis-Mark 1979; Costard 1989; Barlow and Bradley 1990; Barlow and Perez 2003).
2. SLE craters typically range in diameter from ~3 km to 20 km, although they occur over a larger diameter range (both smaller and larger) at high latitudes (Mouginis-Mark 1979; Costard 1989; Barlow and Bradley 1990; Barlow and Perez 2003).
3. The smallest diameter craters showing an SLE morphology (the "onset diameter") range from about 3 km in diameter near the equator to <1 km in diameter near the poles, although regional variations are seen within the equatorial zone (±30° latitude) with onset diameters as low as 1 km in some locations (Kuzmin et al. 1988; Boyce et al. 1998; Barlow et al. 2001).
4. DLE craters are concentrated primarily in topographic lows in the 35–60°N latitude zone, occur in the <3 km to 50 km diameter range, and appear to replace SLE craters within this region (Barlow and Bradley 1990; Barlow and Perez 2003). DLE craters are seen in the corresponding southern hemisphere zone, but in lower concentrations and at higher elevations than those seen in

the north (Barlow and Perez 2003; Boyce and Mouginis-Mark 2005).

5. MLE craters are concentrated within the lower to middle latitude regions, particularly along the hemispheric dichotomy boundary. This morphology is primarily associated with craters in the 15 to 60 km diameter range (Barlow and Bradley 1990; Barlow and Perez 2003).

These layered morphologies often, but not always, terminate in a distal ridge, and are thus also called rampart craters. Other ejecta morphologies observed on Mars include radial (radial pattern similar to that seen around lunar craters), diverse (combination of layered and radial patterns), pancake (no distal rampart), and pedestal (both the crater and ejecta blanket are elevated above the surrounding terrain). Examples of these ejecta types are shown in Fig. 1.

Two major formation models have been proposed to explain the SLE, DLE, and MLE morphologies. One model invokes impact into near-surface volatile reservoirs (Carr et al. 1977; Gault and Greeley 1978; Greeley et al. 1980; Wohletz and Sheridan 1983; Stewart et al. 2001; Stewart and Ahrens 2003), while the other has the ejecta curtain interacting with the thin Martian atmosphere (Schultz and Gault 1979; Schultz 1992a; Barnouin-Jha and Schultz 1998; Barnouin-Jha et al. 1999a, 1999b). Laboratory experiments and numerical modeling have been conducted to demonstrate that both mechanisms can produce many of the features observed with the Martian layered ejecta morphologies (see other papers in this issue). Impact craters on Venus appear to be surrounded by layered ejecta with very large runout distances (Schultz 1992b; Sugita and Schultz 2002), demonstrating the effectiveness of atmospheric-ejecta curtain interactions in producing these ejecta features. Alternately, SLE and DLE patterns are seen on icy moons with little to no atmosphere, such as Ganymede (Passey and Shoemaker 1982; Horner and Greeley 1982; Neal and Barlow 2004) and Europa (Moore et al. 2001). In these cases, the volatile-rich target material must be the major contributor to formation of the observed layered ejecta morphologies. Comparisons of the predicted ejecta characteristics with observations of Martian craters (see review by Barlow 2005) and field observations of terrestrial impact crater ejecta blankets (Hörz et al. 1983; Newsom et al. 1986; Grant and Schultz 1993; Kenkmann and Schönian 2005, 2006; Pope et al. 2005; Stewart et al. 2005) suggest that subsurface volatiles likely play the dominant role in layered ejecta emplacement on Mars, but that the atmosphere may help enhance the emplacement process.

Central pits are another feature commonly seen in Martian impact craters. They have no analogs in the lunar crater population but are common in craters on the icy moons (Passey and Shoemaker 1982; Schenk 1993). The two primary models proposed to explain the central pits are vaporization of subsurface ice during crater formation (Wood et al. 1978) or cometary impacts (Croft 1983). The lack of central pit craters on volatile-poor bodies such as the Moon and Mercury argues against cometary impacts alone being the primary cause of central pit formation. Recent numerical modeling of impacts into ice-soil mixed targets shows that a region under the center of the transient crater cavity reaches high enough temperatures for ice to vaporize (Pierazzo et al. 2005). Both asteroidal and cometary impacts produce this high-temperature region, although the temperatures are higher for cometary impacts due largely to their higher impact velocities. Rapid escape of this vapor could produce the central pits observed on Mars and the icy moons.

Until recently, Viking imagery has served as the primary data source for studies of Martian impact crater characteristics. The Mars Global Surveyor (MGS), Mars Odyssey, and Mars Express (MEx) missions are providing important new insights into the characteristics of Martian impact craters, which can help us better determine how environmental conditions may have influenced the formation of specific ejecta and interior features. MGS's Mars Orbiter Camera (MOC) is providing high-resolution (up to ~2 m/pixel) imagery of the Martian surface in visible wavelengths (Malin and Edgett 2001) and is complemented by Odyssey's Thermal Emission Imaging System (THEMIS) instrument which provides surface views in both visible (VIS; 18 m/pixel resolution) and infrared (IR; 100 m/pixel resolution) wavelengths. THEMIS IR gives important insights into the thermophysical properties of craters and their ejecta blankets (Christensen et al. 2003). MEx's High Resolution Stereo Camera (HRSC) produces imagery in visible wavelengths with resolutions up to 10 m/pixel and is used to produce high-quality stereo views of the surface (Neukum et al. 2005). MGS's Mars Orbiter Laser Altimeter (MOLA) instrument provided the first detailed topographic information for the planet (Smith et al. 2001). MGS's Thermal Emission Spectrometer (TES), Odyssey's THEMIS, and MEx's OMEGA are producing detailed spectral maps which provide information on mineralogic variations within craters and their ejecta blankets (Christensen et al. 2001, 2003; Bibring et al. 2005). MEx's MARSIS instrument has just begun operations but is already providing the first insights into the structure of the upper few kilometers of the Martian substrate (Picardi et al. 2005; Farrell et al. 2005), the region which likely contains the volatile reservoirs into which most of the impact craters are excavating. These new data resources are being used to investigate the characteristics of Martian impact craters in more detail than has previously been possible in an attempt to better understand the role of target volatiles and the atmosphere on the formation of these features.

Catalog of Large Martian Impact Craters

The *Catalog of Large Martian Impact Craters* is a database of impact craters ≥5 km in diameter across the entire surface of Mars. The catalog was compiled from digitization

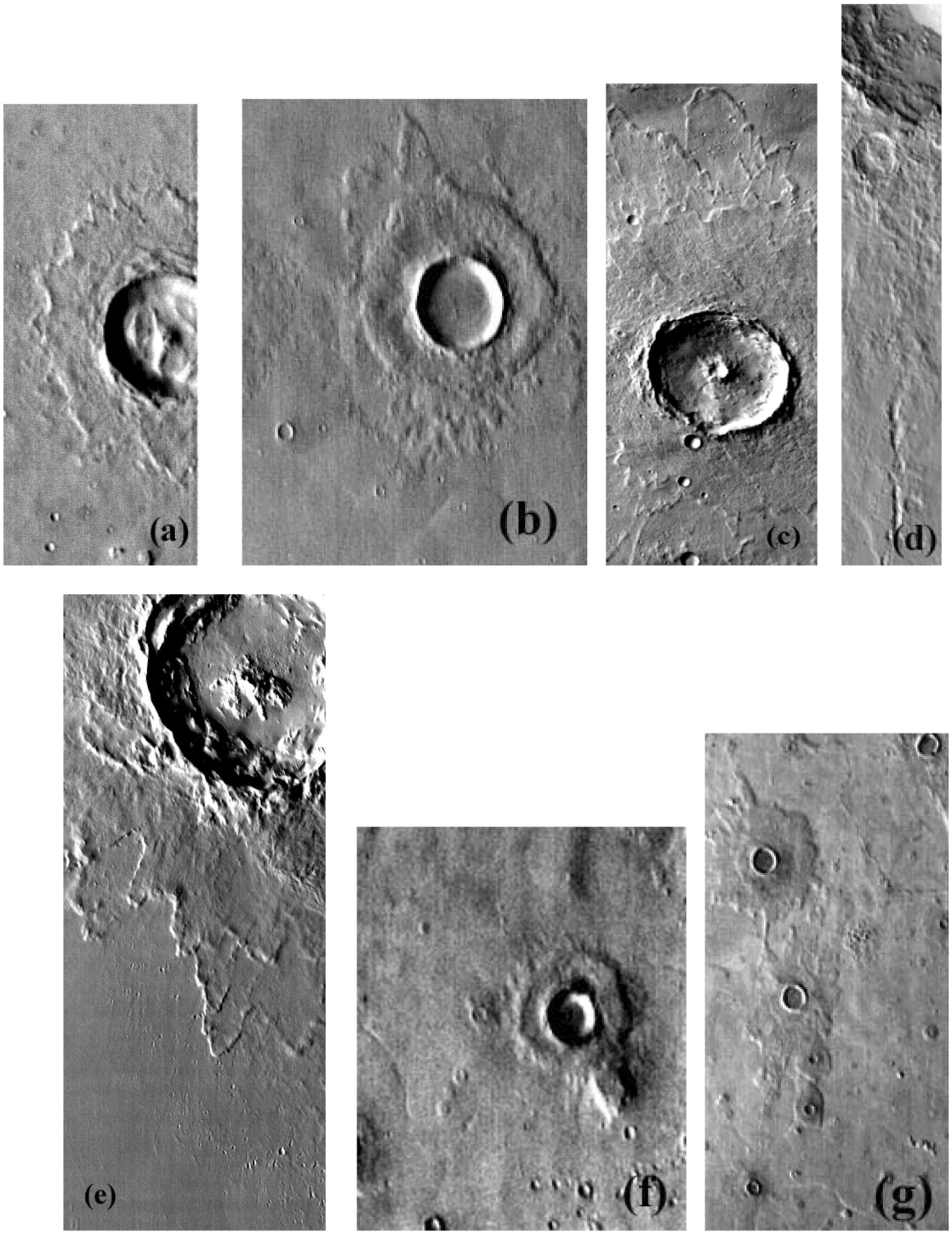

Fig. 1. Examples of ejecta morphologies seen on Mars. a) An SLE crater, 11.6 km in diameter and located at 23.63°N, 101.71°E (THEMIS image I02493005). b) This DLE crater is 6 km in diameter and located at 38.66°N, 93.61°E (THEMIS image I11780004). c) This MLE crater is 22.2 km in diameter and located at 5.73°N, 304.64°E (THEMIS image I03218002). d) Secondary crater chains are common features of the radial ejecta morphology, as shown in the image of a crater 113.3 km in diameter, centered at 28.77°N, 355.22°E. e) Diverse ejecta blankets contain both layered and radial components. This 28.3 km in diameter crater displays secondary crater chains beyond the edge of its layered ejecta morphology. The crater is located at 23.19°N, 207.76°E (THEMIS image I01990002). f) This pancake crater is 3.6 km in diameter and located at 42.41°N, 324.10°E (THEMIS image I11780004). g) Pedestal craters are characterized by the crater and ejecta perched above the surrounding terrain. Pedestal craters often occur in clusters, as shown in this image. The largest crater in this group (upper left side of image) is 3.6 km in diameter and located at 45.97°N, 353.77°E (THEMIS image I12083008).

of the Viking 1:2,000,000-scale photomosaics produced by the U.S. Geological Survey in the 1980s (Barlow 1987). It includes 42,283 craters at all stages of preservation—ranging from extremely fresh to almost completely destroyed ("ghost" craters). Each crater entry contains the following information: MC subquadrangle on which the crater occurs, a crater ID number, latitude and longitude of the crater center, diameter, terrain on which the crater is superposed, general preservational classification ("fresh with ejecta blanket," "modified with no ejecta blanket," "almost destroyed," etc.), ejecta and interior morphologies (if present), minor diameter and azimuthal angle of orientation if crater is elliptical, central pit diameter if applicable, and general comments (typically the crater name if one has been assigned). This crater database (henceforth called Catalog 1.0) has become a premier source of Martian crater information and has been used in studies related to crater-derived chronology studies (Barlow 1988), morphology analyses (Barlow and Bradley 1990), and elliptical crater distributions (Bottke et al. 2000). Catalog 1.0 can be accessed through the U.S. Geological Survey's Planetary Interactive GIS on the Web Analyzable Database (PIGWAD) (http://webgis.wr.usgs.gov).

Catalog 1.0 is currently being revised using MGS MOC and MOLA data and Odyssey THEMIS data (Barlow 2006). Among the changes incorporated into the revised catalog (henceforth called Catalog 2.0) are:

- The latitude and longitude of each crater center are determined from the MOLA-referenced MDIM 2.1.
- All crater diameters are being remeasured and updated as necessary. Obviously elongate craters have both their major and minor diameters measured and their azimuthal angles of orientation determined. Craters which are not highly elongated but which display the "butterfly-type" ejecta pattern indicative of low-angle impacts also have their major diameter, minor diameter, and angle of orientation included.
- The generalized terrain units used in Catalog 1.0 (i.e., "plains," "ridged plains," "cratered plateau," etc.) are replaced with the more commonly used stratigraphic units (Scott and Tanaka 1986; Greeley and Guest 1987; Tanaka and Scott 1987).
- The descriptive preservational class has been replaced by a numeric value ranging from 0.0 ("ghost" crater) to 7.0 (pristine). This value is assigned based on consideration of the measured crater depth and rim height relative to the crater depth and rim height of a fresh crater of similar size, appearance of ejecta and interior features, and average thermal inertia of any existing ejecta blanket relative to the average thermal inertia of the surrounding terrain (see Barlow 2004 for complete description).
- Ejecta and interior morphologies are reevaluated using the new information and updated as necessary. Ejecta morphologies are classified using the nomenclature recommended by the Mars Crater Consortium (Barlow et al. 2000).
- New data in Catalog 2.0 include crater depth and rim height measurements (measured using routines available in JMARS; Gorelick et al. 2003), ejecta extent and geometric characteristics (area and perimeter), ejecta mobility ratio and lobateness (defined in the next section), thermal inertia of surroundings, and general mineralogy of the surroundings.

Catalog 2.0 is approximately 70% complete for the northern hemisphere of Mars, containing updated information on 6795 craters between 0 and 65°N. Three thousand, five hundred, and sixteen of these craters (52%) are degraded to the point where no ejecta blanket is retained. The remaining 3279 craters are associated with some type of ejecta morphology. The analysis reported here emphasizes the morphologic characteristics and distributions of craters displaying ejecta blankets and central pits within the Martian northern hemisphere.

OBSERVATIONS

Single-Layer Ejecta Morphology Craters

Craters displaying the SLE morphology dominate among the layered ejecta morphologies, as noted in the previous Viking-based studies (Mouginis-Mark 1979; Costard 1989; Barlow and Bradley 1990). Of 3279 craters with an ejecta morphology in this study, 1797 (55%) display a SLE morphology. The only regions where SLE craters do not dominate are in the areas where DLE morphology craters are concentrated (see the next section). The SLE morphology is associated with craters whose diameters range from the catalog's lower-diameter cutoff value of 5 km to 41.8 km.

The maximum distance of the ejecta blanket from the crater rim is called the ejecta extent or runout distance and is quantified through the ejecta mobility (EM) ratio (Mouginis-Mark 1979; Costard 1989; Barlow 2004):

$$\mathrm{EM} = \frac{\text{average extent of ejecta blanket from crater rim}}{\text{crater radius}} \quad (1)$$

EM provides information about the fluidity of the ejecta at the time of emplacement. Volatiles from either the atmosphere or vaporized subsurface ice are expected to increase EM, and thus regional variations in EM can provide information about the volatiles in those regions. EM values for SLE craters in the northern hemisphere range between 0.5 and 8.2 with an average value of 1.5. No statistically significant variation is seen between craters on different stratigraphic units. However, a slight trend towards higher EM values is seen with increasing latitude: the mean EM is 1.4 near the equator and rises to 1.7 in the 50–60°N latitude range (Fig. 2).

Lobateness Γ is a measure of the ejecta sinuosity (Kargel 1989; Barlow 1994) and is defined as

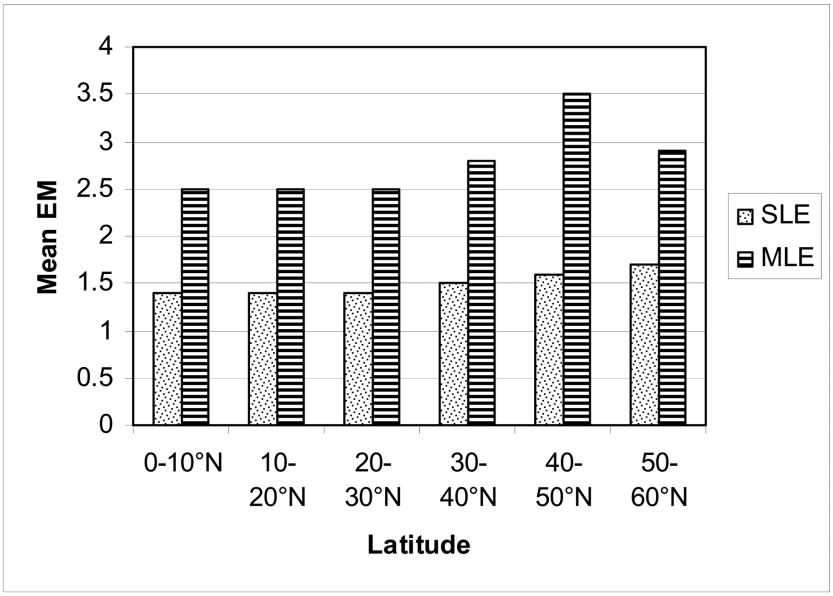

Fig. 2. EM versus latitude. This graph shows the average ejecta mobility (EM) ratio per 10° latitude zone for single-layer and multiple-layer craters in the northern hemisphere. A slight tend towards higher EM with increasing latitude is suggested.

$$\Gamma = \frac{\text{ejecta perimeter}}{[4\pi(\text{ejecta area})]^{1/2}} \quad (2)$$

A circular ejecta blanket will display a lobateness value of 1.0. Higher lobateness values correspond to more sinuous ejecta edges. As with EM, lobateness is thought to be influenced by volatile content and/or the interaction of the ejecta curtain with the atmosphere. From this analysis, we find that Γ varies from 1.00 to 3.45 with a mean value of 1.10 for SLE craters in the northern hemisphere. No statistically significant variations in Γ with latitude or stratigraphic unit are seen.

The SLE morphology typically terminates in a distal rampart for SLE craters in the northern hemisphere. However, at higher latitudes (poleward of ~40°), the number of SLE craters with a pancake (non-rampart) morphology increases. Single-layer pancake ejecta (SLEPn) craters are particularly common in regions where DLE morphology craters dominate and, as discussed in the following section, may be a modified form of DLE craters.

Double-Layer Ejecta and Pancake Morphology Craters

Within the northern hemisphere of Mars, DLE craters have been reported to be concentrated in the topographically low regions of Acidalia, Arcadia, and Utopia Planitia. However, they also occur at higher elevations in the southern hemisphere (Barlow and Perez 2003) so elevation alone does not dictate the location of this morphology. This analysis shows that DLE craters dominate within the 40 to 60°N latitude range and display diameters between 5 km (and smaller) and 115 km. They comprise 28% of the ejecta morphology craters in this study (920 craters).

DLE craters display a number of unique characteristics, including lack of ramparts at the edge of the inner layer and often also for the outer layer, striations on both the inner and outer ejecta layers, and lack of secondary craters beyond the layered ejecta blanket (Boyce and Mouginis-Mark 2005). The inner layer is thicker than the outer layer and, based on stratigraphic evidence, is emplaced before the outer layer (Mouginis-Mark 1981; Mouginis-Mark and Boyce 2005). The runout distance of the outer layer is typically quite large (Mouginis-Mark 1979; Costard 1989) and this outer layer is often quite sinuous (Barlow 1994).

Ejecta mobility ratios for DLE craters show considerable variation between the inner layer and the outer layer. The inner layer displays EM values similar to those of SLE craters in the same latitude zone, with values ranging between 0.4 and 3.0 and an average value of 1.5. The thin outer layer is much more fluid, with an average EM value of 3.3 (range: 1.6 to 9.8). Such large runout distances are difficult to obtain by vaporization of target volatiles alone and suggest that the atmosphere helps to mobilize the flow to these large values, as is seen with crater ejecta flows on Venus (Schultz 1992b; Sugita and Schultz 2002). A base surge origin of the outer ejecta layer has been proposed by Boyce and Mouginis-Mark (2005), which also requires interaction with the atmosphere. The observations are consistent with the results from a study of double-layer craters on Ganymede (an icy body with no significant atmosphere), where outer layer EM values average 1.3, much smaller than those seen on Mars (Neal and Barlow 2004).

No large regional variations in EM are seen, as shown in Table 1. Runout distances of both the inner and outer layers are slightly higher for DLE craters in Arcadia Planitia (30–60°N; ~170–210°E) and Acidalia Planitia (30–60°N;

Table 1. Double-layer ejecta mobility ratios by region.

Region	Location	No. of DLE craters	Mean inner EM	Mean outer EM
Northern Arabia	30–60°N, 0–75°E	179	1.5	3.2
Utopia Planitia	30–60°N, 75–150°E	157	1.4	3.4
Arcadia Planitia	30–60°N, 150–210°E	64	1.7	3.8
Northern Tharsis	30–60°N, 210–300°E	94	1.4	2.9
Acidalia Planitia	30–60°N, 300–360°E	189	1.6	3.6

~305–360°E) than the averages of 1.5 for the inner layer and 3.4 for the outer layer. This suggests that the ejecta curtain was slightly more fluid in these regions during emplacement. The lowest EM values are found for DLE craters in the northern Tharsis volcanic province (30–60°N; 210–300°E), although only the outer layer is statistically below the average.

Lobateness values also vary between the DLE inner and outer layers. The inner layer is typically quite circular, with Γ values having a mean value of 1.09 (range: 1.00–1.40). The outer layer is slightly more sinuous, with values ranging from 1.01 to 2.30 and a mean value of 1.14. These larger EM and Γ values suggests that the ejecta material constituting the outer layer is much more fluid at the time of emplacement than that which forms the inner layer.

Pancake craters (SLEPn) are seen in the same regions where DLE craters dominate. Costard (1989) proposed that SLEPn craters were simply DLE craters where the outer ejecta layer had been destroyed or was unobservable in Viking imagery. From the current analysis, we find strong evidence supporting Costard's proposal. Evidence supporting the hypothesis that SLEPn craters are modified forms of DLE craters includes the following:

- Many craters (in some areas as much as 80%) classified as SLEPn in Catalog 1.0 are now revealed to be DLE craters with the higher resolutions and clearer imagery available in the data being used in Catalog 2.0.
- SLEPn craters are often more degraded than DLE craters.
- The average EM for SLEPn craters is 1.6, very similar to the mean value of 1.5 for the inner layer of DLE craters.
- The mean Γ value of 1.06 for SLEPn is statistically identical to the mean Γ value of 1.09 for the DLE inner layer.

Multiple-Layer Ejecta Morphology Craters

Multiple-layer craters account for 506 of the 3279 craters with ejecta morphologies in this study (15%). They range in diameter from 5.6 to 90.7 km, but are most common at diameters greater than 10 km. The improved image resolutions of the MGS and Odyssey data allow the MLE morphology to be seen around smaller craters than has been previously reported from Viking analysis (Barlow and Bradley 1990).

MLE craters display two or more partial or complete ejecta layers. Typically, only the outermost ejecta layer completely encircles the crater. We therefore compute EM and Γ values only for this outermost layer. The EM range is between 1.2 and 5.4, but the average values increase from 2.5 within the 0–30°N latitude zone to >3.5 at latitudes >40°N (Fig. 2). Lobateness values range between 1.02 and 1.64, with a median value of 1.25. The number of MLE craters drops off dramatically at latitudes poleward of ~35°, occurring only around craters >30 km in diameter above 50°N.

Pedestal Craters

Pedestal (Pd) craters are unique landforms on Mars where both the crater and ejecta blanket are elevated above the surrounding terrain. These craters are concentrated in the northern mid-latitude zone which previous studies have found to be covered by fine-grained deposits (e.g., Soderblom et al. 1974) (Fig. 3). Arvidson et al. (1976) suggested that pedestal craters form when the material surrounding the crater's ejecta blanket is deflated by eolian processes. The rough, competent surface of the ejecta essentially shields the underlying surface from this erosion. Although the exact mechanism by which this armoring occurs is not understood, terrestrial landslides typically show a coarse carapace overlying finer-grained material (McSaveney 2005), and something similar might occur in these ejecta blankets. Alternately, copious amounts of melt are produced by impacts into volatile-rich material (Stewart and Ahrens 2005), and analog studies of terrestrial craters reveal that the proximal ejecta deposits often contain large amounts of this melt (Osinski 2006). Thus impact melt might provide the armoring mechanism. In any event, Arvidson et al.'s (1976) model argues that eolian deflation removes the fine-grained material surrounding the Pd crater, leaving both the crater and ejecta blanket perched above the surrounding terrain. A major problem with the eolian model is that the Pd ejecta is typically quite symmetrical, which requires a changing preferential wind direction over the entire 360° area around the crater to produce the observed morphology.

Most Pd craters are quite small, typically <6 km in diameter (Fig. 1g). They are not included in this analysis because they are below the lower-diameter cutoff of 5 km for the catalog. However, in a separate study, we have characterized Pd craters down to ~0.5 km in diameter, as revealed in MOC and THEMIS imagery (Kadish and Barlow 2006). That analysis has identified 1027 pedestal craters within the 0–60°N latitude zone, with most located north of 35°N (Fig. 3), within the same region where DLE and SLEPn

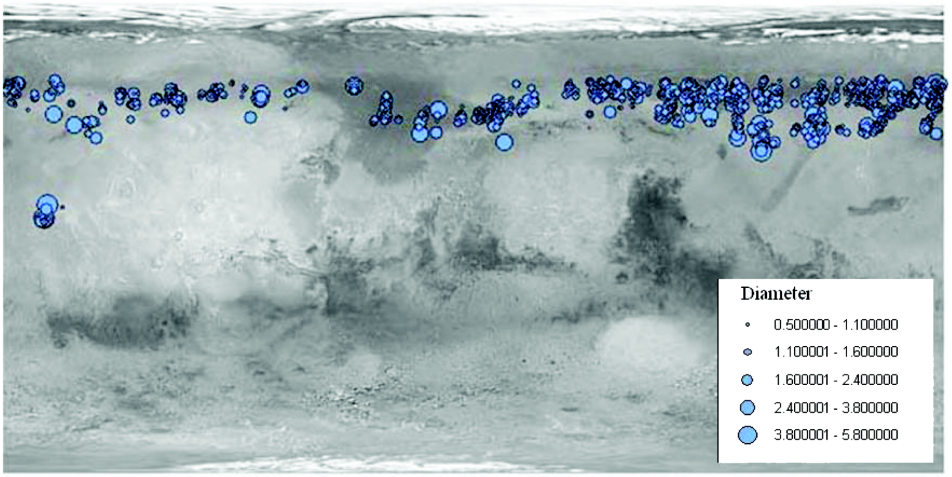

Fig. 3. This map shows the distribution of Pd craters in the northern hemisphere of Mars. Circle size reflects the diameter ranges of Pd craters. Most Pd crates are located in the 35–60°N latitude zone. The only grouping of Pd craters existing outside of this region occurs in the fine-grained deposits of the Medusae Fossae Formation.

are concentrated. Smaller pedestal craters are seen at higher latitudes. The only low-latitude concentration of Pd craters occurs in the Medusae Fossae Formation just west of the Tharsis region where thick fine-grained deposits are found. Pd craters have some of the highest EM values, ranging from 1.2 to 13.2 with a mean of 3.3. Lobateness values range between 1.00 and 2.50 (mean = 1.10). The highest EM and Γ values are found for craters in the Medusae Fossae Formation and in the eastern Utopia Planitia region, north of Elysium Mons.

Central Pit Craters

Craters with central pits fall into three categories: those with symmetric pits on their floors (SY; "symmetric floor pits"), those with asymmetric pits on their floors (AP; "asymmetric floor pits"), and those with pits raised above the floor, often on top of a central peak (SP; "summit pits") (Fig. 4). Barlow and Bradley's (1990) Viking-based analysis identified central pits in craters with diameter ranges between 16 and 64 km, with SP craters dominating at lower crater diameters (16–32 km), SY occurring in intermediate-size craters (32–45 km), and AP dominating in the larger craters (45–64 km). They also noted that central pits tend to be concentrated along the proposed outer rings of large impact basins, suggesting that terrain properties such as the concentration of ice along ring fractures might be implicated in the formation of central pits.

The current study finds that central pits occur in smaller craters than those reported by Barlow and Bradley (1990) and do not show as strong of a diameter dependence as previously reported. Our results find that SY occur in craters between 5.2 and 114.0 km in diameter while AP and SP overlap this range (9.7–62.5 km and 6.1–57.0 km, respectively). SY comprise 76% of the 373 central pits surveyed to date; SP follow at 22% and AP are the rarest (2%). Regional variations in central pit occurrence do not correlate with specific pit types-regions which show asymmetric pits also show summit and symmetric floor pits in the same diameter range. The analysis of central pit distributions is not complete enough at this point to determine if the correlation of pits with proposed basin rings still holds, but this analysis does show high concentrations of central pits from southern Lunae Planum through the western side of Arabia Terra, along the boundaries of proposed basins in Chryse Planitia (Schultz et al. 1982) and Arabia Terra (Dohm et al. 2004).

Symmetric floor pits are seen in craters within the entire latitude range of this study (0–65°N). SP craters extend up to 46°N while AP are only observed at latitudes <40°N. Most pits are associated with craters fresh enough to still retain an ejecta blanket (preservational classes 4.0–7.0), but a few are associated with craters that are old enough that the ejecta blanket has been destroyed (preservation classes as old as 1.0). As shown in Table 2, SY and SP mainly occur in craters which display an MLE morphology, suggesting that the conditions favoring MLE formation also preferentially produce central pits.

The ratio of the central pit diameter to the diameter of the parent crater is generally consistent among all three central pit types. The ratio of the pit diameter to the crater diameter (D_p/D_c) ranges between 0.07 and 0.24 for SY craters, with an average of 0.15. AP craters display a D_p/D_c range of 0.07 to 0.18, with an average of 0.13, and SP craters have a range of 0.04 to 0.19, with an average of 0.12. These values are statistically identical and suggest that once the conditions for central pit formation are met, they do not vary considerably among central pit type.

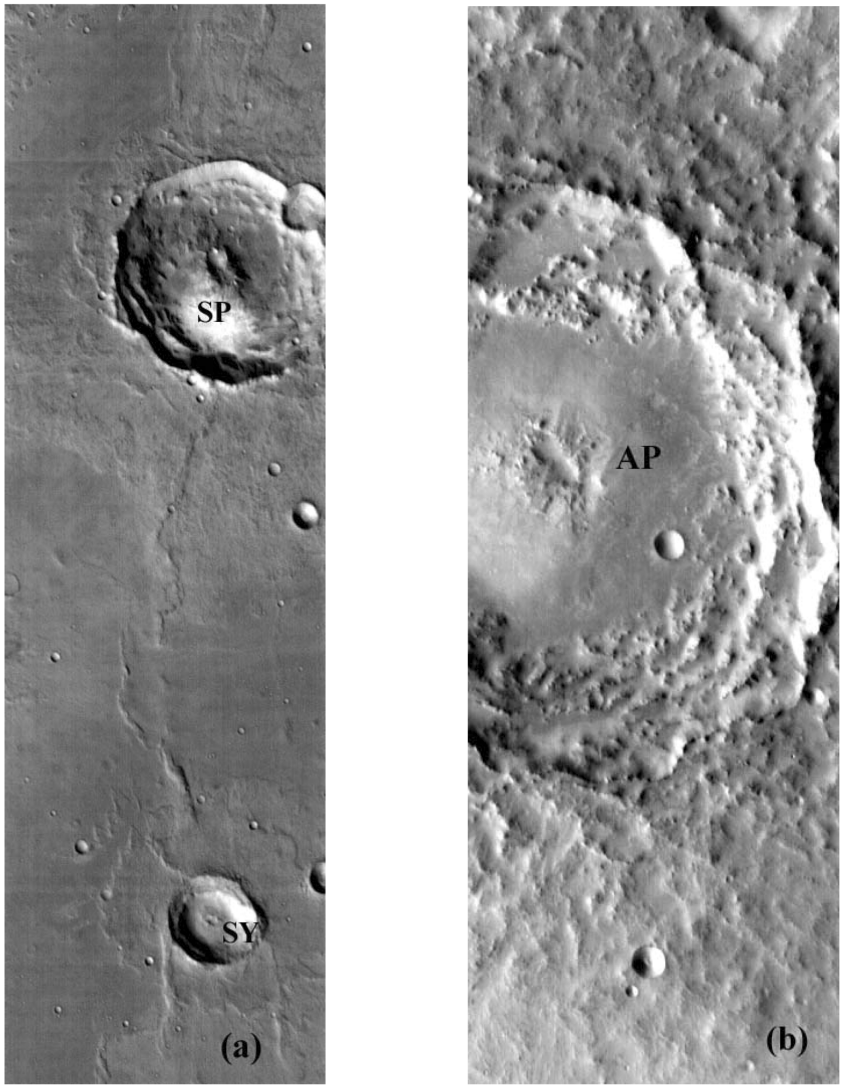

Fig. 4. Central pit craters. Central pits are classified into three types. a) Symmetric floor pits (SY) are the most common type of central pit seen on Mars and are similar in many respects to the floor pits seen in craters on icy Ganymede. Summit pits (SP) are pits elevated above the crater floor, often on top of a central peak. Summit pits are the second most common pit feature on Mars but have no analogs in central pit craters on Ganymede. The SP crater near the top is 22.6 km in diameter and located at 17.78°N, 308.98°E, while the SY crater near the bottom is 9.8 km in diameter and located at 16.71°N, 308.81°E (THEMIS image I101250013). b) Asymmetric floor pits (AP) comprise only 2% of all central pits cataloged to date. This AP crater is 50.9 km in diameter and located at 20.18°N, 69.39°E (THEMIS image I10383012).

DISCUSSION

Revision of the *Catalog of Large Martian Impact Craters* using MGS and Odyssey data has resulted in both confirmation of and changes to our understanding of impact craters in the northern hemisphere of Mars based on earlier analyses of the Viking data. This analysis continues to show that SLE craters are the dominant layered ejecta morphology in most regions on Mars. The SLE morphology primarily occurs around craters up to ~20 km in diameter within the 0–30°N latitude range and around craters up to ~42 km in diameter at higher latitudes. EM values are roughly constant throughout this region, with only a slight trend towards higher values at higher latitudes. Lobateness values are also relatively constant throughout the northern hemisphere. Thermal inertia values cover a range from low (24 J m^{-2} $s^{-1/2}$ K^{-1}) to intermediate (up to ~400 J m^{-2} $s^{-1/2}$ K^{-1}) throughout the regions where SLE craters are found (Jakosky et al. 2000; Putzig et al. 2005), suggesting that variations in surface material properties do not contribute significantly to SLE properties such as EM and Γ. Similarly, SLE craters occur at all elevations within the northern hemisphere, ranging from 21 km in elevation at Olympus Mons to −5 km in Utopia Planitia (Smith et al. 2001). The atmospheric model for SLE formation argues that variations in atmospheric pressure and the distribution of fine-grained material will produce

differences in the SLE morphology. These are not seen in the morphology, EM, or Γ values of SLE craters in the northern hemisphere of Mars.

The other model for SLE formation invokes impact into and vaporization of subsurface volatiles. Numerical modeling suggests that this mechanism can reproduce many of the observed attributes of the SLE morphology (Stewart et al. 2001; Stewart and Ahrens 2003). The excavation depth (d_e) of impact craters (i.e., the maximum depth reached during transient crater formation) can be estimated from their observed rim diameters (D_a) using the following (Garvin et al. 2000):

$$d_e = 0.131 D_a^{0.85} \quad (3)$$

Using this relationship, we find that SLE craters are excavating to depths of ~1.7 km near the equatorial region (for $D \approx 20$ km) and to depths of ~3 km at higher latitudes (for $D_a = 42$ km). While the ejecta material is derived from only approximately the top 1/3 of this depth (Melosh 1989), deeper volatiles can be vaporized during crater formation and contribute to the vapor plume which produces the layered ejecta morphology. Thus, these excavation depths can be considered averages for the depth of the subsurface volatiles. These depths are within the expected ice-rich regions of the Martian substrate based on geothermal and hydrologic models (Clifford 1993). The smallest crater diameter at which the SLE morphology is seen decreases poleward (Kuzmin et al. 1988), which is consistent with the theoretical models which predict ice closer to the surface at higher latitudes (Clifford 1993) as well as the neutron spectrometer data from the Mars Odyssey mission (Feldmann et al. 2004). The low variability in EM and Γ suggests that the ice content within the upper 3 km does not vary considerably throughout the northern plains nor has it varied considerably over the time scales recorded by these craters (Barlow 2004). All of the observations of SLE craters are consistent with impact into ice-rich target materials being the dominant formation process.

Northern hemisphere DLE craters are seen over a similar size range as the SLE craters but are strongly concentrated in the 35–60°N latitude zone. While the strongest concentrations of DLE craters are seen in topographically low regions which contain large amounts of fine-grained material (Soderblom et al. 1974; Jakosky et al. 2000; Putzig et al. 2005), they also are seen at higher elevations with higher thermal inertia values. This suggests that elevation and/or fine-grained surface material are not the sole contributors to the DLE morphology, as has been previously proposed (Costard 1994; Barlow and Perez 2003). Morphologic analysis of DLE craters using THEMIS and MOC imagery suggests that the ejecta was emplaced in two stages, with the inner layer emplaced first by a process similar to SLE emplacement (Boyce and Mouginis-Mark 2005). The outer layer occurs later with a slow-moving (<100 m/s) base surge. This is consistent with the observations from this study which show that the inner layer has EM and Γ values similar to SLE craters, and especially single-layer pancake craters, in the same regions. The outer DLE layer has one of the largest average runout distance of any ejecta type, as indicated by the average EM value of 3.3 (but with values as high as 9.8). DLE craters tend to occur within the ice-rich mantling deposit, believed to have been emplaced during the last high obliquity period (Mustard et al. 2001). The proposed high ice content of these materials may contribute excess vapor to the ejecta, resulting in higher mobilization of the ejected material. However, DLE craters on ice-rich Ganymede do not show such large runout distances for their outer layers (Neal and Barlow 2004). This suggests that the Martian atmosphere combined with the excess vapor from the target materials helps to fluidize the DLE outer layer (Schultz 1992b; Sugita and Schultz 2002).

Table 2. Central pits versus ejecta morphology.

Ejecta morphology	SY	AP	SP
SLE	72 (25%)	2 (22%)	20 (25%)
DLE	27 (10%)	2 (22%)	4 (5%)
MLE	157 (55%)	3 (33%)	53 (66%)
No ejecta	28 (10%)	2 (22%)	3 (4%)
Total craters	284	9	80

Multiple-layer craters in the northern hemisphere are seen over a wider range of diameters than was reported from Viking-based analysis. Again, there is no strong correlation of MLE craters with elevation or thermal inertia, although there is a trend towards MLE craters being concentrated along the hemispheric dichotomy boundary, as previously reported by Barlow and Perez (2003). The large EM and Γ values associated with the outer complete ejecta layer suggests that the ejecta is highly fluid during emplacement. One model for MLE craters is that they excavate into liquid water reservoirs (Wohletz and Sheridan 1983; Barlow and Bradley 1990). The depths to which these craters excavate vary from 0.5 (D = 5.6 km) to 6 km (D = 107 km). Most MLE craters are excavating to ~2–3 km depth within the equatorial region, well within the region where liquid water may be present according to geothermal models (Clifford 1993). However, the smaller craters are excavating to depths much shallower than where liquid water is expected and the high latitude craters, even though they tend to be larger than MLE craters in the equatorial region, are excavating to depths where liquid water would not be expected at these near-polar latitudes. Unless there is considerable heterogeneity in the distribution of subsurface groundwater reservoirs, another formation mechanism must be considered. No MLE craters are observed on icy Ganymede (Neal and Barlow 2004), suggesting that the atmosphere may play a role in MLE formation on Mars. Wind tunnel experiments and numerical modeling suggest that larger impacts will develop more complicated vortices within the atmosphere, which could produce the numerous

partial layers observed with MLE craters (Barnouin-Jha et al. 1999a, 1999b). However, the regional variations in MLE distribution suggest that target properties still play some role, as does the observation that the smallest MLE craters often occur at higher elevations (Lunae Planum, eastern Arabia) and within regions where other strong evidences of near-surface volatiles (such as channels) occur. As with the DLE outer layer, we suspect that vaporization of near-surface volatile-rich materials contributes to and enhances the effects of the Martian atmosphere, with the latter likely varying in density with climate changes initiated by variations in obliquity and orbital properties (Head et al. 2003).

Pedestal craters in the Martian northern hemisphere are largely located in the mid-latitude ice-rich mantling deposit where DLE and SLEPn craters are also concentrated. The average Pd EM value of 3.3 is higher than for SLE craters (mean = 1.5) and comparable to the EM for the outer DLE layer (mean = 3.3). This implies that the ejecta was highly mobile during emplacement. Pd craters have low sinuosity, with a mean $\Gamma = 1.10$. These results are consistent with the hypothesis that Pd craters form by impact into ice-rich, fine-grained materials which covered this region during previous high obliquity periods (Mustard et al. 2001; Head et al. 2003). We propose that sublimation of this ice, rather than eolian deflation, is responsible for the Pd crater morphology. The craters formed entirely in this ice-rich mantle during higher obliquity periods and armoring of the ejecta blanket occurred. As Mars moves towards lower obliquity, ice begins to sublimate from this mantle deposit, with higher amounts of sublimation occurring at lower latitudes, as indicated by the slightly larger Pd craters seen between 35 and 45°N. As the ice sublimates, the surrounding terrain is lowered, leaving the crater and its armored ejecta blanket elevated above the surroundings. Based on the size of the largest Pd crater (~6 km) and its estimated excavation depth of ~1 km, we estimate that sublimation has lowered the surroundings by up to 1 km. Similarities in Pd EM and Γ values with those of the outer DLE layer suggest that Pd craters are the small crater equivalent of DLE craters. DLE craters do not show the pedestal effect since they have excavated through the thin mantling deposit and the subsequent lowering of the surroundings does not produce an obvious pedestal morphology for these deeper craters.

Central pit craters are more common and occur over a larger diameter range than previously reported. There is currently no obvious correlation of the three central pit types with diameter, contrary to previous studies (Barlow and Bradley 1990). Hydrocode models of impacts into soil-ice mixed targets shows that a vapor zone is produced near the center of most transient craters (Pierazzo et al. 2005). Sudden release of this vapor could produce the central pit morphology, but why some pits are on the crater floor while others are raised is not currently understood. It is also unclear why some craters produce central pits when nearby, similarly aged craters which show layered ejecta blankets and other indicators of subsurface volatiles do not have pits. Further analysis of central pit craters in the southern hemisphere may help to clarify the environmental conditions under which these pits form.

SUMMARY OF CONCLUSIONS

The present study of Martian northern hemisphere craters is consistent with target volatiles playing a dominant role in the formation of central pits and the layered ejecta morphologies. Sublimation of an ice-rich mantle deposited at mid-latitudes during previous high obliquity periods is consistent with the observed distribution and characteristics (size, ejecta mobility ratios, and lobatnesses) of pedestal craters in the northern hemisphere. While ejecta curtain interactions with the thin Martian atmosphere help to explain the large runout distances of the DLE and MLE, vapor produced during impact into volatile-rich targets likely enhances the atmospheric component. Thus, the latest observations of Martian impact crater characteristics in the northern hemisphere of Mars continue to support the premise that many of the features associated with these craters are the result of impact into a volatile-rich crust.

Acknowledgments–This research was supported by NASA Mars Data Analysis Program grants NAG5-8265 and NAG5-12510. The author thanks Robert Craddock and Joseph Boyce for constructive reviews.

Editorial Handling—Dr. A. J. Timothy Jull

REFERENCES

Arvidson R. E., Coradini M., Carusi A., Coradini A., Fulchignoni M., Federico C., Funiciello R., and Salomone M. 1976. Latitudinal variation of wind erosion of crater ejecta deposits on Mars. *Icarus* 27:503–516.

Barlow N. G. 1987. Relative ages and the geologic evolution of Martian terrain units. Ph.D thesis, The University of Arizona, Tucson, Arizona, USA.

Barlow N. G. 1988. Crater size-frequency distributions and a revised Martian relative chronology. *Icarus* 75:285–305.

Barlow N. G. 1994. Sinuosity of Martian rampart ejecta deposits. *Journal of Geophysical Research* 99:10,927–10,935.

Barlow N. G. 2004. Martian subsurface volatile concentrations as a function of time: Clues from layered ejecta craters. *Geophysical Research Letters,* doi:10.1029/2003GL019075.

Barlow N. G. 2005. A review of Martian impact crater ejecta structures and their implications for target properties. In *Large meteorite impacts III,* edited by Kenkmann T., Hörz F., and Deutsch A. Boulder, Colorado: Geological Society of America. pp. 433–442.

Barlow N. G. 2006. Status report on the *Catalog of Large Martian Impact Craters*, version 2.0 (abstract #1337). 37th Lunar and Planetary Science Conference. CD-ROM.

Barlow N. G. and Bradley T. L. 1990. Martian impact craters: Correlations of ejecta and interior morphologies with diameter, latitude, and terrain. *Icarus* 87:156–179.

Barlow N. G. and Perez C. B. 2003. Martian impact crater ejecta

morphologies as indicators of the distribution of subsurface volatiles. *Journal of Geophysical Research,* doi:10.1029/2002JE002036.

Barlow N. G., Koroshetz J., and Dohm J. M. 2001. Variations in the onset diameter for Martian layered ejecta morphologies and their implications for subsurface volatile reservoirs. *Geophysical Research Letters* 28:3095–3098.

Barlow N. G., Boyce J. M., Costard F. M., Craddock R. A., Garvin J. B., Sakimoto S. E. H., Kuzmin K. O., Roddy D. J., and Soderblom L. A. 2000. Standardizing the nomenclature of Martian impact crater ejecta morphologies. *Journal of Geophysical Research* 105:26,733–26,738.

Barnouin-Jha O. S. and Schultz P. H. 1998. Lobateness of impact ejecta deposits from atmospheric interactions. *Journal of Geophysical Research* 103:25,739–25,756.

Barnouin-Jha O. S., Schultz P. H., and Lever J. H. 1999a. Investigating the interactions between an atmosphere and an ejecta curtain. 1. Wind tunnel tests. *Journal of Geophysical Research* 104:27,105–27,115.

Barnouin-Jha O. S., Schultz P. H., and Lever J. H. 1999b. Investigating the interactions between an atmosphere and an ejecta curtain. 2. Numerical experiments. *Journal of Geophysical Research* 104:27,117–27,131.

Bottke W. F., Love S. G., Tytell D., and Glotch T. 2000. Interpreting the elliptical crater populations on Mars, Venus, and the Moon. *Icarus* 145:108–121.

Boyce J. M. and Mouginis-Mark P. J. 2005. Martian craters viewed by the THEMIS instrument: Double-layered ejecta craters (abstract). Workshop on the Role of Volatiles and Atmospheres on Martian Impact Craters. pp. 27–28.

Boyce J. M., Roddy D. J., and Soderblom L. A. 1998. Distribution of onset diameters of rampart ejecta craters on Mars (abstract #1404). 29th Lunar and Planetary Science Conference. CD-ROM.

Bribing J.-P., Langevin Y., Gendrin A., Gondet B., Poulet F., Berthé M., Soufflot A., Arvidson R., Mangold N., Mustard J., and Drossart P. 2005. Mars surface diversity as revealed by the OMEGA/Mars Express observations. *Science* 307:1576–1581.

Carr M. H., Crumpler L. S., Cutts J. A., Greeley R., Guest J. E., and Masursky H. 1977. Martian impact craters and emplacement of ejecta by surface flow. *Journal of Geophysical Research* 82: 4055–4065.

Christensen P. R., Bandfield J. L., Hamilton V. E., Ruff S. W., Kieffer H. H., Titus T. N., Malin M. C., Morris R. V., Lane M. D., Clark R. L., Jakosky B. M., Mellon M. T., Pearl J. C., Conrath B. J., Smith M. D., Clancy R. T., Kuzmin R. O., Roush T., Mehall G. L., Gorelick N., Bender K., Murray K., Dason S., Greene E., Silverman S., and Greenfield M. 2001. Mars Global Surveyor Thermal Emission Spectrometer experiement: Investigation description and surface science results. *Journal of Geophysical Research* 106:23,823–23,872.

Christensen P. R., Bandfield J. L., Bell J. F., Goerelick N., Hamilton V. E., Ivanov A., Jakosky B. M., Kieffer H. H., Lane M. D., Malin M. C., McConnochie T., McEwen A. S., McSween H. Y., Mehall G. L., Moersch J. E., Nealson K. H., Rice J. W., Richardson M. I., Ruff S. W., Smith M. D., Titus T. N., and Wyatt M. B. 2003. Morphology and composition of the surface of Mars: Mars Odyssey THEMIS results. *Science* 300:2056–2061.

Clifford S. M. 1993. A model for the hydrologic and climatic behavior of water on Mars. *Journal of Geophysical Research* 98: 10,973–11,016.

Costard F. M. 1989. The spatial distribution of volatiles in the Martian hydrolithosphere. *Earth, Moon, and Planets* 45:265–290.

Costard F. M. 1994. Unusual concentrations of rampart craters at the mouths of outflow channels, Mars (abstract). 25th Lunar and Planetary Science Conference. pp. 287–288.

Croft S. K. 1983. A proposed origin for palimpsests and anomalous pit craters on Ganymede and Callisto. *Journal of Geophysical Research* 88:B71–B89.

Dohm J. M., Barlow N., Williams J.-P., Baker V. R., Anderson R. C., Boynton W. V., Fairén A. G., and Hare T. M. 2004. Ancient giant impact basin/aquifer system in the Arabia region, Mars (abstract #1209). 35th Lunar and Planetary Science Conference. CD-ROM.

Farrell W. M., Plaut J. J., Gurnett D. A., and Picardi G. 2005. Detecting subglacial aquifers in the north polar layered deposits with Mars Express/MARSIS. *Geophysical Research Letters,* doi: 10.1029/2005GL022488.

Feldman W. C., Prettyman T. H., Maurice S., Plaut J. J., Bish D. L., Vaniman D. T., Mellon M. T., Metzger A. E., Squyres S. W., Karunatillake S., Boynton W. V., Elphic R. C., Funsten H. O, Lawrence D. J., and Tokar R. L. 2004. Global distribution of near-surface hydrogen on Mars. *Journal of Geophysical Research,* doi:10.1029/2003JE002160.

Garvin J. B., Sakimoto S. E. H., Frawley J., and Schnetzler C. 2000. North polar region crater forms on Mars: Geometric characteristics from the Mars Orbiter Laser Altimeter. *Icarus* 144:329–352.

Gault D. E. and Greeley R. 1978. Exploratory experiments of impact craters formed in viscous-liquid targets: Analogs for Martian rampart craters? *Icarus* 34:486–495.

Gorelick N. S., Weiss-Malik M., Steinberg B., and Anwar S. 2003. JMARS: A multimission data fusion application (abstract #2057). 34th Lunar and Planetary Science Conference. CD-ROM.

Grant J. A. and Schultz P. H. 1993. Erosion of ejecta at Meteor Crater, Arizona. *Journal of Geophysical Research* 98:15,033–15,047.

Greeley R., Fink J., Gault D. E., Snyder D. B., Guest J. E., and Schultz P. H. 1980. Impact cratering in viscous targets: Laboratory experiments. Proceedings, 11th Lunar and Planetary Science Conference. pp. 2075–2097.

Greeley R. and Guest J. E. 1987. Geologic map of the eastern equatorial region of Mars. Scale: 1:15,000,000. USGS Miscellaneous Investigator Map I-1802-B.

Head J. W., Mustard J. F., Kreslavsky M. A., Milliken R. E., and Marchant D. R. 2003. Recent ice ages on Mars. *Nature* 426:797–802.

Horner V. M. and Greeley R. 1982. Pedestal craters on Ganymede. *Icarus* 51:549–562.

Hörz F., Ostertag R., and Rainey D. A. 1983. Bunte Breccia of the Ries: Continuous deposits of large impact craters. *Reviews of Geophysics and Space Physics* 21:1667–1725.

Jakosky B. M., Mellon M. T., Kieffer H. H., Christensen P. R., Varnes E. S., and Lee S. W. 2000. The thermal inertia of Mars from the Mars Global Surveyor Thermal Emission Spectrometer. *Journal of Geophysical Research* 105:9643–9652.

Kadish S. J. and Barlow N. G. 2006. Pedestal crater distribution and implications for a new model of formation (abstract #1254). 37th Lunar and Planetary Science Conference. CD-ROM.

Kargel J. S. 1989. First and second-order equatorial symmetry of Martian rampart crater ejecta morphologies (abstract). The Fourth International Conference on Mars. pp. 132–133.

Kenkmann T. and Schönian F. 2005. Impact craters on Mars and Earth: Implications by analogy (abstract). Workshop on the Role of Volatiles and Atmospheres on Martian Impact Craters. pp. 57–58.

Kenkmann T. and Schönian F. 2006. Ries and Chicxulub: Impact craters on Earth provide insights for Martian ejecta blankets. *Meteoritics & Plantary Science* 41. This issue.

Kuzmin R. O., Bobina N. N., Zabalueva E. V., and Shashkina V. P. 1988. Structural inhomogeneities of the Martian cryosphere. *Solar System Research* 22:121–133.

Malin M. C. and Edgett K. S. 2001. Mars Global Surveyor Mars Orbiter Camera: Interplanetary cruise through primary mission. *Journal of Geophysical Research* 106:23,429–23,570.

McSaveney M. J., and Davies T. R. H. 2005. Making a grain-bridge connection between two rocky planets (abstract). Workshop on the Role of Volatiles and Atmospheres on Martian Impact Craters. pp. 73–74.

Melosh H. J. 1989. *Impact cratering: A geologic process*. New York: Oxford University Press. 253 p.

Moore J. M., Asphaug E., Belton M. J. S., Bierhaus B., Breneman H. H., Brooks S. M., Chapman C. R., Chuang F. C., Collins G. C., Giese B., Greeley R., Head J. W., Kadel S., Klaasen K. P., Klemaszewski J. E., Magee K. P., Moreau J., Morrison D., Neukum G., Pappalardo R. T., Phillips C. B., Schenk P. M., Senske D. A., Sullivan R. J., Turtle E. P., and Williams K. K. 2001. Impact features on Europa: Results of the Galileo Europa mission (GEM). *Icarus* 151:93–111.

Mouginis-Mark P. 1979. Martian fluidized ejecta morphology: Variations with crater size, latitude, altitude, and target material. *Journal of Geophysical Research* 84:8011–8022.

Mouginis-Mark P. J. 1981. Water or ice in the Martian regolith? Clues from rampart craters seen at very high resolution. *Icarus* 71:268–286.

Mouginis-Mark P. J. and Boyce J. M. 2005. The unique attributes of Martian double layered ejecta craters (abstract #1111). 36th Lunar and Planetary Science Conference. CD-ROM.

Mustard J. F., Cooper C. D., and Rifkin M. K. 2001. Evidence for recent climate change on Mars from the identification of youthful near-surface ground ice. *Nature* 412:411–414.

Neal J. E. and Barlow N. G. 2004. Layered ejecta craters on Ganymede: Comparisons with Martian analogs (abstract #1121). 35th Lunar Planetary Science Conference. CD-ROM.

Neukum G. and the HRSC Co-Investigator Team 2005. The High Resolution Stereo Camera (HRSC) experiment on Mars Express: Highlight results from observations over one and a half years in orbit (abstract). *Bulletin of the American Astronomical Society* 37:656.

Newsom H. E., Graup G., Sewards T., and Keil K. 1986. Fluidization and hydrothermal alteration of the suevite deposit at the Ries crater, West Germany, and implications for Mars. *Journal of Geophysical Research* 91:E239–E251.

Osinski G. R. 2006. Effect of volatiles and target lithology on the generation and emplacement of impact crater fill and ejecta deposits on Mars. *Meteoritics & Plantary Science* 41.This issue.

Passey Q. R. and Shoemaker E. M. 1982. Craters and basins on Ganymede and Callisto: Morphological indicators of crustal evolution. In *Satellites of Jupiter,* edited by Morrison D. Tucson, Arizona: The University of Arizona Press. pp. 379–434.

Picardi G., Plaut J. J., Biccari D., Bomboci O. Calabrese D., Cartacci M., Cicchetti A., Clifford S. M., Edenhofer P., Farrell W. M., Federico C., Frigeri A., Gurnett D. A., Hagfors T., Heggy E., Herique A., Huff R. L., Ivanov A. B., Johnson W. T. K., Jordan R. L., Kirchner D. L., Kofman W., Leuschen C. J., Nielson E., Orosei R., Pettinelli E., Phillips R. J., Plettemeier D., Safaeinili A., Seu R., Stofan E. R., Vannaroni G., Watters T. R., and Zampolini E. 2005. Radar soundings of the subsurface of Mars. *Science* 310:1925–1928.

Pierazzo E., Artemieva N. A., and Ivanov B. A. 2005. Starting conditions for hydrothermal systems underneath Martian craters: Hydrocode modeling. In *Large meteorite impacts III,* edited by Kenkmann T., Hörz F., and Deutsch A. Boulder, Colorado: Geological Society of America. pp. 443–457.

Pope K. O., Ocampo A. C., Fischer A. G., Vega F. J., Ames D. E., King D. T., Fouke B. W., Wachtman R. J., and Kletetschka G. 2005. Chicxulub impact ejecta deposits in southern Quintana Roo, Mexico, and central Belize. In *Large meteorite impacts III,* edited by Kenkmann T., Hörz F., and Deutsch A. Boulder, Colorado: Geological Society of America. pp. 171–190.

Putzig N. E., Mellon M. T., Kretke K. A., and Arvidson R. E. 2005. Global thermal inertia and surface properties of Mars from the MGS mapping mission. *Icarus* 173:325–341.

Schenk P. M. 1993. Central pit and dome craters: Exposing the interiors of Ganymede and Callisto. *Journal of Geophysical Research* 98:7475–7498.

Schultz P. H. 1992a. Atmospheric effects on ejecta emplacement. *Journal of Geophysical Research* 97:11,623–11,662.

Schultz P. H. 1992b. Atmospheric effects on ejecta emplacement and crater formation on Venus from Magellan. *Journal of Geophysical Research* 97:16,183–16,248.

Schultz P. H. and Gault D. E. 1979. Atmospheric effects on Martian ejecta emplacement. *Journal of Geophysical Research* 84:7669–7687.

Schultz P. H., Schultz R. A., and Rogers J. 1982. The structure and evolution of ancient impact basins on Mars. *Journal of Geophysical Research* 87:9803–9820.

Scott D. H. and Tanaka T. L. 1986. Geologic map of the western equatorial region of Mars. Scale: 1:15,000,000. USGS Miscellaneous Investigator Map I-1802-A.

Soderblom L. A., Condit C. D., West R. A., Herman B. M., and Kreidler T. J. 1974. Martian planetwide crater distributions-Implications for geologic history and surface processes. *Icarus* 22:239–263.

Smith D. E., Zuber M. T., Frey H. V., Garvin J. B., Head J. W., Muhleman D. O., Pettengill G. H., Phillips R. J., Solomon S. C., Zwally H. J., Banerdt W. B., Duxbury T. C., Golombek M. P., Lemoine F. G., Neumann G. A., Rowlands D. D., Aharonson O., Ford P. G., Ivanov A. B., Johnson C. L., McGovern P. J., Abshire J. B., Afzal R. S., and Sun X. 2001. Mars Orbiter Laser Altimeter: Experiment summary after the first year of global mapping of Mars. *Journal of Geophysical Research* 106: 23,689–23,722.

Stewart S. T. and Ahrens T. J. 2003. Shock Hugoniot of H_2O ice. *Geophysical Research Letters*, doi:10.1029/2002GL016789.

Stewart S. T. and Ahrens T. J. 2005. Shock properties of H_2O ice. *Journal of Geophysical Research,* doi:10.1029/2004JE0902305.

Stewart S. T., O'Keefe J. D., and Ahrens T. J. 2001. The relationship between rampart crater morphologies and the amount of subsurface ice (abstract #2092). 32nd Lunar and Planetary Science Conference. CD-ROM.

Stewart S. T., Louzada K. L., Maloof A. C., Newsom H. E., Weiss B. P., and Wright S. P. 2005. Field observations of ground-hugging ejecta flow at Lonar crater, India (abstract #1273). Workshop on the Role of Volatiles and Atmospheres on Martian Impact Craters. pp. 102–103.

Sugita S. and Schultz P. H. 2002. Initiation of run-out flows on Venus by oblique impacts. *Icarus* 155:265–284.

Tanaka K. L. and Scott D. H. 1987. Geologic map of the polar regions of Mars. Scale: 1:15,000,000. USGS Miscellaneous Investigator Map I-1802-C.

Wohletz K. H. and Sheridan M. F. 1983. Martian rampart crater ejecta: Experiments and analysis of melt-water interactions. *Icarus* 56:15–37.

Wood C. A., Head J. W., and Cintala M. J. 1978. Interior morphology of fresh Martian craters: The effects of target characteristics. Proceedings, 9th Lunar and Planetary Science Conference. pp. 3691–3709.